

UC Santa Barbara

UC Santa Barbara Previously Published Works

Title

Integrated hybrid silicon DFB laser-EAM array using quantum well intermixing

Permalink

<https://escholarship.org/uc/item/6541m10p>

Journal

Optics Express, 19(14)

Authors

Jain, Siddharth
Sysak, Matthew
Kurczveil, Geza
et al.

Publication Date

2011-06-30

Peer reviewed

Integrated hybrid silicon DFB laser-EAM array using quantum well intermixing

Siddharth R. Jain,^{1,*} Matthew N. Sysak,² Geza Kurczveil,¹ and John E. Bowers¹

¹Department of Electrical Engineering, University of California, Santa Barbara, California 93106, USA

²Photonics Technology Labs, Intel Corporation, Santa Clara, California 95054, USA

*siddharth@ece.ucsb.edu

Abstract: We demonstrate multiple bandgap integration on the hybrid silicon platform using quantum well intermixing. A broadband DFB laser array and a DFB-EAM array are realized on a single chip using four bandgaps defined by ion implantation enhanced disordering. The broadband laser array uses two bandgaps with 17 nm blue shift to compensate for gain roll-off while the integrated DFB-EAMs use the as-grown bandgap for optical gain and a 30 nm blue shifted bandgap for modulation. The multi-channel DFB array includes 13 lasers with >90 nm gain-bandwidth. The transponder includes four DFB-EAMs with 14 dB DC extinction at 4 V bias.

©2011 Optical Society of America

OCIS codes: (140.2010) Diode laser arrays; (230.4110) Modulators.

References and links

1. H. Park, A. W. Fang, D. Liang, Y.-H. Kuo, H.-H. Chang, B. R. Koch, H.-W. Chen, M. N. Sysak, R. Jones, and J. E. Bowers, "Photonic integration on the hybrid silicon evanescent device platform," *Adv. Opt. Technol.* **2008**, 682978 (2008).
2. H. H. Chang, Y. H. Kuo, R. Jones, A. Barkai, and J. E. Bowers, "Integrated hybrid silicon triplexer," *Opt. Express* **18**(23), 23891–23899 (2010).
3. M. N. Sysak, J. O. Anthes, J. E. Bowers, O. Raday, and R. Jones, "Integration of hybrid silicon lasers and electroabsorption modulators," *Opt. Express* **16**(17), 12478–12486 (2008).
4. E. Skogen, J. Raring, G. Morrison, C. Wang, V. Lal, M. Masanovic, and L. Coldren, "Monolithically integrated active components: a quantum-well intermixing approach," *IEEE J. Sel. Top. Quantum Electron.* **11**(2), 343–355 (2005).
5. G. Lin and C. Lee, "Comparison of 1300 nm quantum well lasers using different material systems," *Opt. Quantum Electron.* **34**(12), 1191–1200 (2002).
6. D. Liang and J. Bowers, "Highly efficient vertical out gassing channels for low-temperature InP-to-silicon direct wafer bonding on the silicon-on-insulator (SOI) substrate," *J. Vac. Sci. Technol. B* **26**(4), 1560–1568 (2008).
7. J. W. Raring, "Advanced InP based monolithic integration using quantum well intermixing and MOCVD regrowth," Ph. D dissertation, Department of Electrical and Computer Engineering, University of California, Santa Barbara. June 2006.
8. Y. H. Kuo, H. W. Chen, and J. E. Bowers, "High speed hybrid silicon evanescent electroabsorption modulator," *Opt. Express* **16**(13), 9936–9941 (2008).
9. Y. Tang, H. Chen, S. Jain, J. Peters, U. Westergren, and J. Bowers, "50 Gb/s hybrid silicon travelling-wave electroabsorption modulator," *Opt. Express* (to be published).

1. Introduction

A CMOS manufacturing-compatible laser source holds the key to realize integrated silicon photonics based devices for optical communication and optical computing. Heterogeneous integration by direct wafer bonding of a III-V active region to pre-patterned silicon-on-insulator (SOI) waveguides has been successfully demonstrated as a promising technology to address this challenge. This technique utilizes III-V material for optical gain/modulation and silicon for optical wave-guiding and does not require any alignment during bonding. Using taper structures, the evanescent optical mode between the III-V and silicon can be completely transferred to the SOI waveguide, enabling integration with other silicon based optical devices. Using this approach, a variety of discrete devices such as distributed feedback (DFB) and distributed Bragg reflector (DBR) lasers, electro-absorption modulators (EAMs), and photodetectors (PDs) have been demonstrated [1]. However, demonstrations of more complex

photonic circuits have been limited by the number of III-V bandgaps that can be generated without the use of multiple bonding steps or complicated epitaxial structures [2].

In [3] quantum well intermixing (QWI) was used as a technique for integration on the hybrid silicon platform to demonstrate a single SGDBR (Sampled Grating Distributed Bragg Reflector) laser - EAM integration at 1.5 μm wavelength. Ion implantation enhanced disordering was used to generate three bandgaps using a single growth and single bond step. In this work we extend the same approach to higher levels of integration and demonstrate a broadband thirteen channel DFB laser array and a four channel DFB-EAM transponder array on a single chip, targeted at short-reach interconnect applications in the 1.3 μm wavelength range. A total of four bandgaps - two for lasers, one for EAMs and one for passive sections - spread over 60 nm are generated across a single chip. Two laser bandgaps separated by 17 nm are used to realize the broad band optical source on silicon with gain bandwidth of >90 nm from 1255 to 1345 nm. A laser bandgap and an EAM bandgap separated by 30 nm are used to realize the integrated transponder with 3 dB bandwidth of 2 GHz.

2. Quantum well intermixing, the technology

The intermixing technology used in this work is based on ion implantation enhanced disordering [4]. The base structure used for QWI is shown in Fig. 1(a). The structure consists of 7x6.5 nm wide, 0.8% compressively strained InGaAsP wells with 8x8 nm wide 0.3% tensile strained InGaAsP barriers. The QW structure was designed with constant group III composition as we expect the change in bandgap per unit change in atomic concentration to be larger for group V elements [5]. To increase confinement factor and decrease distance of vacancy propagation from the top buffer, the quantum well (QW) structure is asymmetrically placed directly below the super-lattice with a 250 nm thick separate confinement heterostructure (SCH) layer on the other side. The epi structure is otherwise similar to that used for previous demonstrations on the hybrid platform with the addition of a top InP buffer layer and a InGaAsP stop-etch layer.

Intermixing begins with a blanket phosphorous ion implant into the InP buffer layer to generate vacancies (Fig. 1(a)). A SiON_x cap masks sections of the III-V wafer from the implant, preserving the as-grown bandgap (#1). Rapid thermal anneal at 725 $^\circ\text{C}$ diffuses these

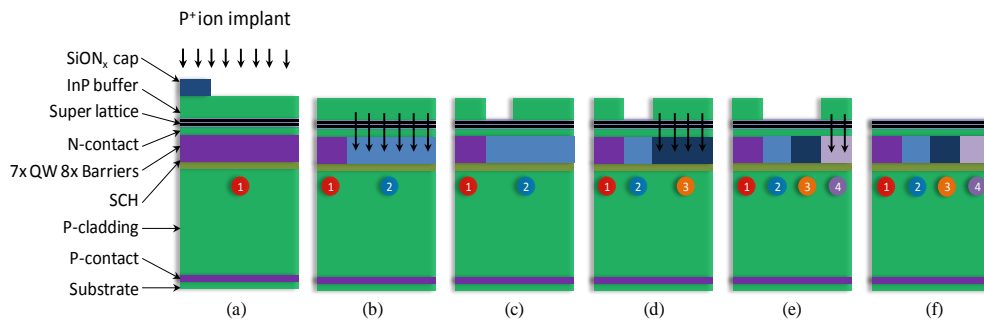


Fig. 1. Overview of ion implantation based quantum well intermixing process used for the hybrid silicon platform. Four bandgap regions defined across the wafer are numbered 1, 2, 3 and 4. (a) Phosphorous ion implant into InP buffer with SiON_x mask to preserve as-grown bandgap 1. (b) Diffusion of vacancies through quantum wells and barriers during RTA to create bandgap 2. (c) Selective removal of InP buffer layer to stop intermixing. (d) Diffusion of vacancies through QW structure for bandgap 3. (e) Selective removal of InP buffer and anneal for bandgap 4. (f) Blanket removal of InP buffer layer to planarize surface.

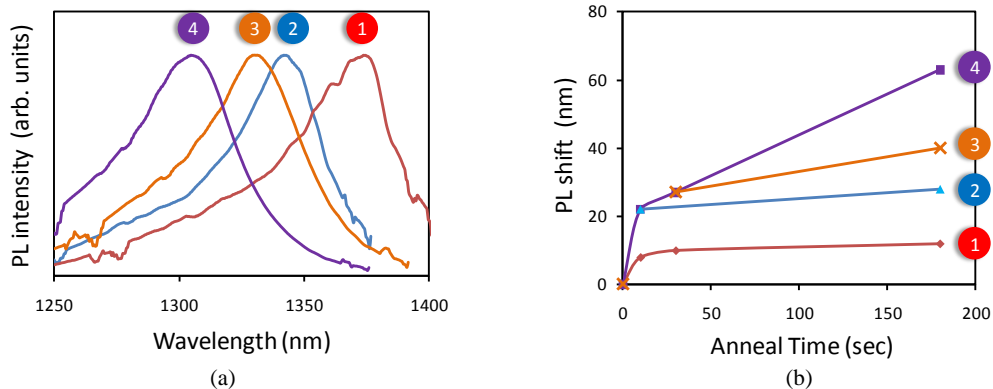


Fig. 2. (a) Normalized PL spectra obtained from four bandgaps across the wafer. (b) PL shift as a function of RTA time for four bandgaps across the wafer.

vacancies into the QW structure below, initiating atomic inter-diffusion between the wells and barriers that modifies the compositional and potential profile and hence creating bandgap 2 (Fig. 1(b)).

By selectively etching the buffer layer over certain regions of the wafer, the source of defects/vacancies can be removed, thereby slowing down the intermixing process (Fig. 1(c)). This allows for control on the level of intermixing undergone by certain areas of the wafer. Additional annealing is then used to continue the bandgap shifting in the regions where the InP buffer remains (Fig. 1(d)). Thus by using multiple anneal steps and selectively removing the buffer layer between the anneal cycles, multiple bandgaps can be generated across the wafer (Fig. 1(e)). As the final step after multiple bandgap definitions, the InP buffer and InGaAsP stop-etch layers are blanket wet etched to planarize the surface (Fig. 1(f)).

The implant energy and dosage of phosphorus ions used was 100 keV and $5 \times 10^{14} \text{ cm}^{-2}$ respectively. The implant energy was set to confine the defects in the top InP buffer layer and the dosage was optimized on the basis of PL shift and PL intensity. It should be noted that phosphorus ions are electrically inactive and do not reach the QWs during the implant. The anneal time and temperature was selected to achieve maximum net PL shift possible (PL shift in implanted region - PL shift in un-implanted region) while maintaining the film quality of the wafer. A dielectric stack of PECVD based low stress SiON_x - SiO_2 - SiON_x (3x40 nm) was developed to prevent surface degradation during the anneal cycles. The samples were encapsulated on the front and backside to prevent InP decomposition. Due to strain compensation between the tensile SiON_x and compressive SiO_2 films, the dielectric did not crack during the annealing and a planar surface was retained to allow for planar surface-to-surface bonding later in the fabrication process.

Normalized photoluminescence (PL) spectra from the four bandgap regions on the chip are shown in Fig. 2(a). Figure 2(b) is a plot of the PL shift as a function of RTA time for the III-V epi wafer used in this work. Two laser bandgaps - corresponding to #1 and #2 and an EAM bandgap (#3) along with a passive bandgap (#4) for the taper regions are defined with anneal time of 10, 20 and 150 sec. Compared to the as-grown material, the first laser bandgap (#1) is shifted by 10 nm (PL peak at 1357 nm), the second laser bandgap (#2) by 27 nm (1340 nm), EAM bandgap (#3) by 40 nm (1327 nm) and the passive bandgap (#4) by 63 nm (1304 nm).

3. Device fabrication

Device fabrication is divided into three parts: pre-bond, bonding and post-bond steps.

Pre-bond steps include fabrication of SOI waveguides, selective area intermixing, realization of deep-etch backside alignment marks and definition of gratings. Waveguides and

vertical channels [6] are fabricated on 0.4 μm Si height SOI wafers. The thickness of the oxide layer is 1 μm . Waveguide width and etch depth is set to 0.8 and 0.3 μm respectively

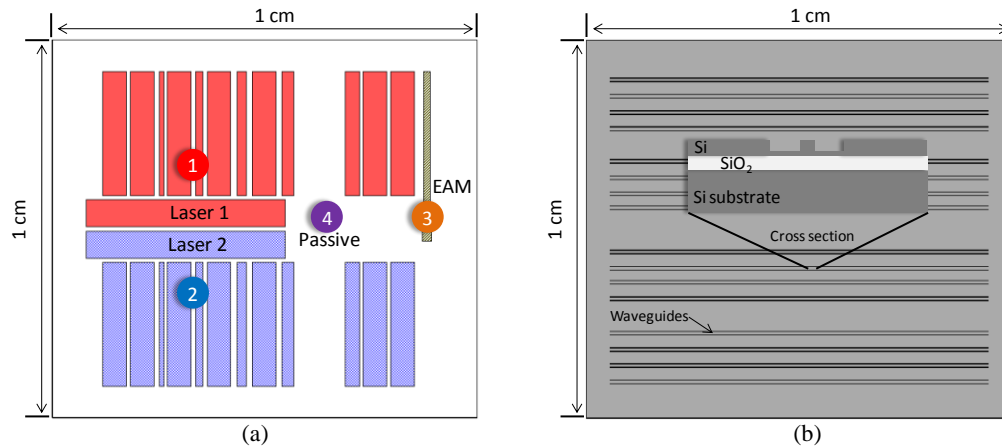


Fig. 3. Schematic of patterned (a) III-V and (b) SOI wafer after pre-bond fabrication steps. Four bandgaps defined across III-V wafer are labeled 1, 2, 3 and 4 representing two laser bandgaps, an EAM and passive bandgap respectively. III-V wafer patterns have a stripe-like geometry in vertical direction and SOI waveguides are continuous in the horizontal direction.

based on optimization of mode profile for confinement factor and lateral width of the mode in the QWs. FIMMWAVE simulations estimate a confinement factor of 5% in the QWs.

As shown in Fig. 3(a), stripes of laser (#1 & #2) and EAM (#3) bandgaps are patterned on the III-V wafer and the rest is shifted to the passive bandgap (#4). Each bandgap definition, as illustrated earlier in Fig. 1, involves passivation, rapid thermal anneal and selective removal of the top InP buffer over areas defining that particular bandgap. Stripes of active bandgaps (#1 & #2) are used to define lasers and PDs, while the passive sections (#4) are used to define tapers or proton-implanted isolation sections between lasers and PDs. Next, a set of alignment marks are etched through the wafer and into p-contact layer stopping right before the substrate. Finally, arrays of quarter-wave shifted gratings with different pitches are defined in the supper lattice layer of the III-V wafer using electron-beam lithography.

A plasma-assisted bonding process [1] is used to bond the patterned SOI and III-V wafers. Introduction of intermixing to the hybrid silicon laser fabrication process translates to patterning III-V wafer before bond step, thus necessitating alignment of the III-V to SOI wafer during bonding. Substrate removal after bonding exposes the deeply etched alignment marks and these are used to measure the alignment error of III-V wafer with respect to exposed markers on Si. Using a MA-8 flip-chip aligned bonder, a rotational alignment of $<0.1^\circ$ and translational alignment of $< \pm 7 \mu\text{m}$ was repeatedly achieved. Due to the striped geometry of patterns on both III-V and SOI wafers (Fig. 3), translational alignment is not critical and small errors can be accounted for by setting an offset parameter in the following lithography steps. However, rotational alignment is critical to ensure that the waveguides in Si are perpendicular to the gratings on III-V. This requirement can be relaxed by defining gratings in Si instead of III-V.

Post bond processing is similar to that in [1] and [3]. Steps include definition of ridge mesa and tapers, contacts to p- and n-layers, n-layer etch under p-probe metal to reduce parasitic capacitance, proton implantation and probe metallization. The dies are diced, polished and AR coated prior to testing.

4. Device design

Two sets of lasers with 300 and 500 μm (L_a) long active sections are fabricated over both the laser bandgaps (#1 & 2). Gratings are etched in the inner 100, 150 μm (L_g) of the 300 and 500

μm long lasers respectively. Each set has fifteen different grating periods corresponding to lasing wavelengths from 1255 to 1370 nm. Gratings are 20 nm deep and the grating strength, kappa 'k', simulated using film mode matching (FMM) method is about 400 cm^{-1} . To avoid a large ' kL_g ' value, the grating length (L_g) was intentionally set to be lower than the active device length (L_a). All lasers are integrated with 500 μm long backside PDs at the same bandgap as the laser for on-chip characterization as shown in Fig. 4. The detectors also double up as backside absorbers. Adjacent lasers and PDs are isolated using 20 μm long proton implanted regions which are shifted to the passive bandgap. As depicted in the cross section in Fig. 5, lasers have a 20 μm wide mesa and a 4 μm wide current channel that is defined using proton implantation. The laser, PD and passive section cross-sections are structurally identical with the only difference in that the passive section does not have a current channel or metal contacts.

Integrated EAMs are 100 μm long with a 4 μm wide mesa to reduce capacitance and are connected to the wider laser section with a proton implanted taper. A 150 μm long taper following the EAM is used to transition the optical mode from the III-V to the Si. All taper sections remain unpumped and are defined using the passive bandgap (Fig. 6). The option to realize passive tapers is an inherent advantage of using quantum well intermixing on the hybrid silicon platform as they are less absorbing and do not need to be electrically pumped. Figure 7 is an image of the fabricated chip with the integrated DFB array and DFB-EAM transponder array.

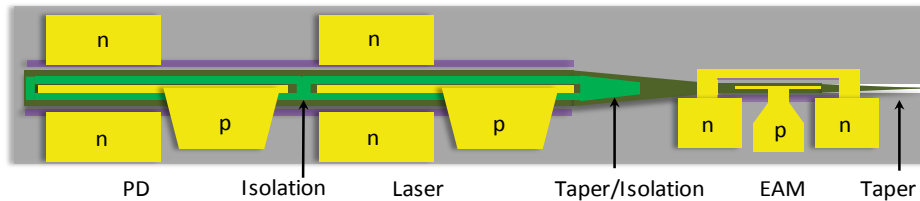


Fig. 4. Schematic top view of integrated DFB-EAM transmitter with backside photodetector. Devices are interconnected with isolation and taper sections.

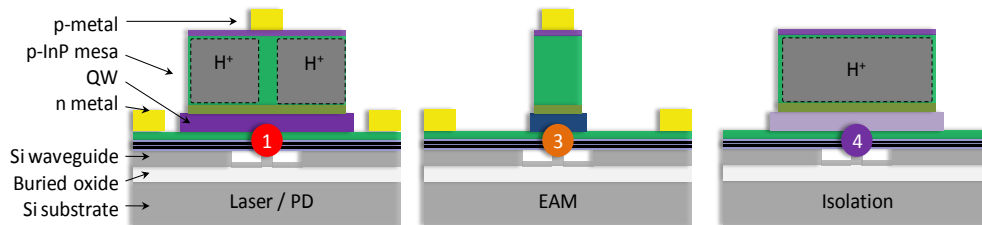


Fig. 5. Schematic cross section of (a). Laser/photodetector section (bandgap 1, PL = 1357 nm, bandgap 2, PL = 1340 nm). (b) EAM with narrow 4 μm mesa (bandgap 3, PL = 1327 nm) (c). Isolation section (bandgap 4, PL = 1304 nm).

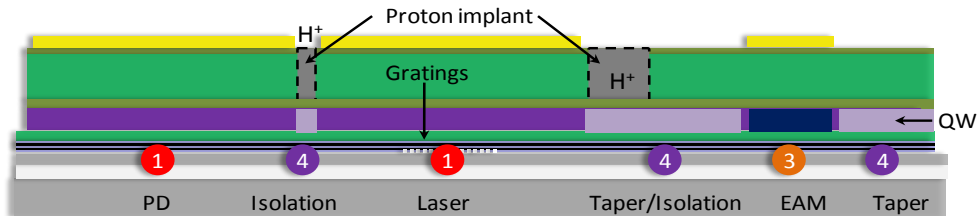


Fig. 6. Schematic side view of integrated DFB-EAM transmitter with backside photodetector. Three bandgaps used are numbered 1, 3 and 4 (laser, EAM and passive) and depicted with different shades for the quantum well region. Gratings are defined over inner 100/150 μm for 300/500 μm long DFB lasers.

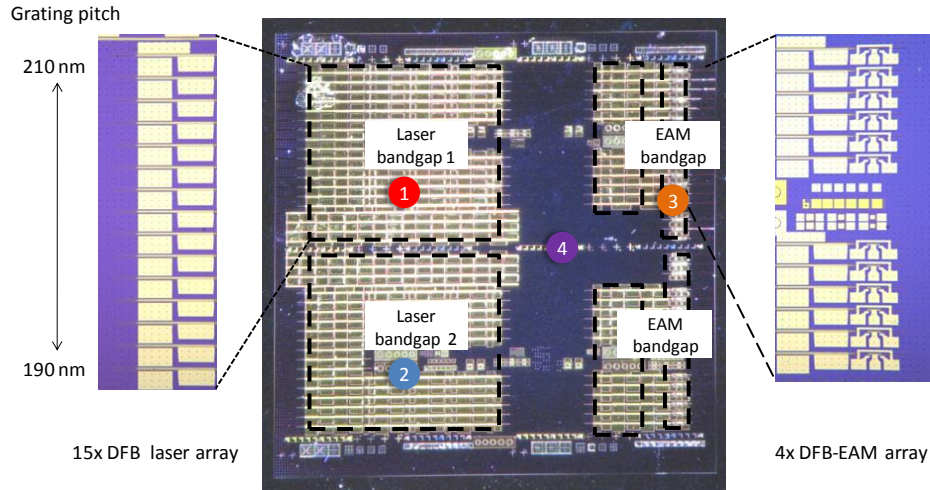


Fig. 7. Top view of fabricated chip. Four bandgaps regions defined across the wafer are marked. To the left is a zoomed in image of 15 DFB laser array with varying grating pitch. Similar laser arrays are defined using laser bandgaps (#1 & #2). Integrated DFB-EAM array are on the right edge of the chip and utilize the EAM bandgap (#3) for modulation.

5. Device performance

5.1 Multi channel DFB laser array

CW LI characteristic of a typical 500 μm long DFB in the laser array is shown in Fig. 8(a). CW operation is achieved up to 60 $^{\circ}\text{C}$ with 4 mW single side output power at 20 $^{\circ}\text{C}$ and a threshold current of 40 mA. Output power is measured with the integrated backside photodetector assuming ideal responsivity. Damage to Si waveguides that couple light out of the chip prevented measurement of actual output power from the lasers and responsivity characterization of the detectors. Large kappa value of the gratings and the effect of setting $L_g < L_a$ potentially contribute to the low extraction efficiency and low output power. Thorough study of threshold and power variation with grating strength and design is required to study and improve laser performance. An inset of the DFB laser spectra is also shown in Fig. 8(a). Side mode suppression ratio for all DFB lasers is above 40 dB. Figure 8(b) plots the variation in threshold for all operational 300 μm lasers with the lasing wavelength using either bandgap 1 or 2 as the gain medium. Lasers over one bandgap (#1) could operate over 60 nm (1280 to 1340 nm), with threshold variation from 50 to 125 mA, but with an additional bandgap (#2)

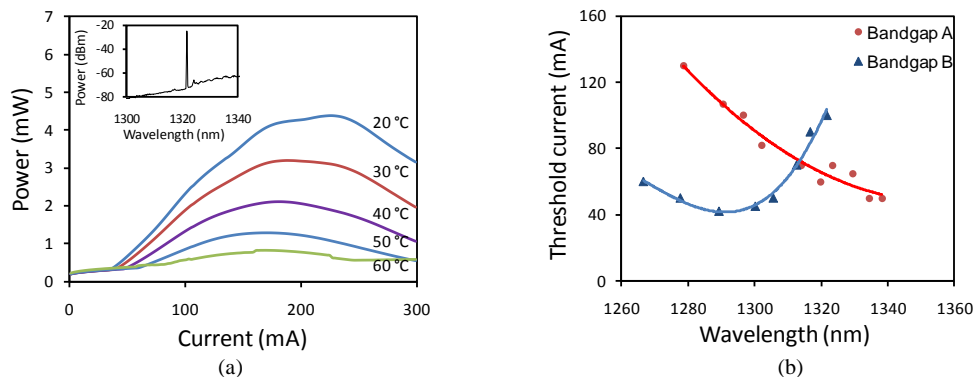


Fig. 8. (a) CW LI characteristics of 500 μm DFBs measured using the on-chip backside photodetector, assuming ideal conversion. (b) Variation of threshold current with lasing wavelength of 300 μm long DFBs.

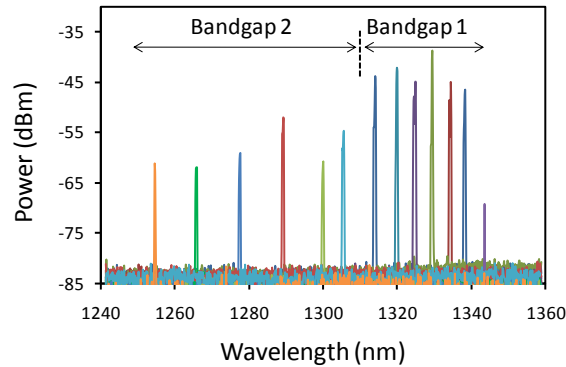


Fig. 9. Collective spectra of thirteen DFB lasers selected from lasers over bandgap A and B with 40-70 mA threshold current.

to compensate for gain roll-off, operating wavelength range can be increased to 75 nm with smaller variation in threshold current (40-70 mA). Figure 9 plots the collective lasing spectra of all functioning 300 and 500 μm long DFBs over bandgap 1 and 2 with threshold current between 40 and 70 mA. For grating periods corresponding to 1255 and 1345 nm, spectra from the 500 μm cavity devices are shown. For wavelengths above 1255 and below 1345 nm, spectra from the 300 μm DFB cavity devices are shown. Lasers operating with bandgap 2 span from 1255 to 1310 nm and those with bandgap 1 from 1310 to 1345 nm. We thus have thirteen DFBs operating over a 90 nm bandwidth. Due to lack of working devices with grating pitch corresponding to wavelengths above 1340 nm, threshold plot could not be extended beyond 1340 nm but the general trend in threshold from Fig. 8(b) suggests that the actual operating range with 40-70 mA threshold is greater than 100 nm. Spectra are not evenly spaced due to grating design and device damage during facet polish. Damage to Si waveguides near the facet explains the random variation in power levels in Fig. 9.

5.2 Integrated DFB-EAM transponder

The integrated hybrid silicon transponder includes the above mentioned lasers integrated with EAMs. DC extinction characteristic for the EAMs at 10, 30 and 50 nm detuning, as tested with an external source is shown in Fig. 10(a). Extinction ratio of 14 dB is achieved with a bias voltage of -4 V at 30 nm detuning. The sharp drop in extinction ratio with bias can be attributed to the shape of the quantum wells after intermixing and smaller than optimal detuning between the laser and modulator band edge which can be corrected for with larger PL shift [7]. Insertion loss of the EAM was not measured during damage to test structures during fabrication.

Small signal electrical to optical (EO) bandwidth measurement results for the integrated EAMs are shown in Fig. 10(b). The 3-dB bandwidth of these devices was 2 GHz, which is in close agreement with what is expected using the measured device resistance of 13 Ω and associated capacitance of 1.5 pF. The EO response is currently limited by the parasitic capacitance associated with the probe metal pads, and can be extended to 10 GHz with the addition of low-K dielectric and smaller metal pads for reduced capacitance [8]. By using travelling wave electrode designs and increasing the number of wells the bandwidth can potentially be further pushed to 40 GHz [9].

6. Summary

We have demonstrated quantum well intermixing based integration for devices that require multiple bandgaps in the hybrid silicon platform. Four bandgaps were generated on a single

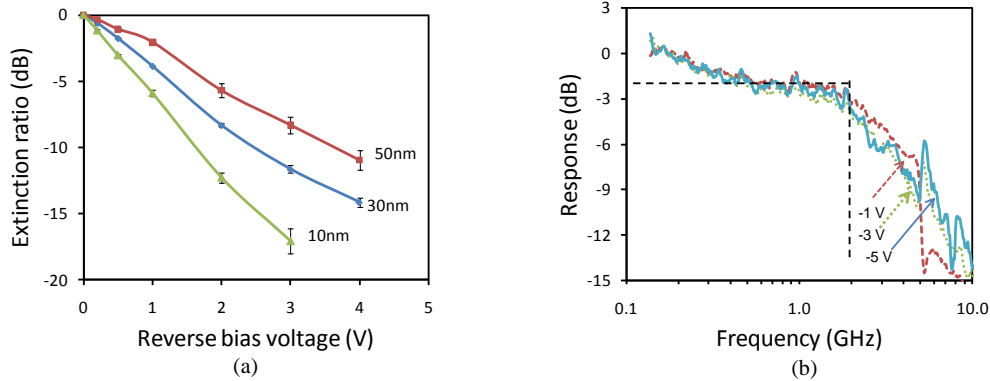


Fig. 10. (a) Measured DC extinction ratio for integrated EA modulators. 14 dB extinction is achieved with -4 V bias for 30 nm detuning. (b) Small signal bandwidth measurement results for the integrated EA modulators. Bias voltages are -1 , -3 , and -5 V as indicated.

chip and used to realize a multi-channel DFB laser array and DFB lasers integrated with EAMs. Thirteen CW operational DFB lasers with 40-70 mA threshold current and four-channel DFB-EAM array with 2 GHz bandwidth were fabricated. Device performance needs to be improved through careful design but this work nonetheless serves to demonstrate the feasibility of multiple bandgap integration on this platform.

Acknowledgments

The authors would like to thank Anand Ramaswamy, Hui-Wen Chen, Molly Piels, Di Liang and Erica Lively for valuable discussions and help with device fabrication and testing. This work was supported by Intel Corp. under Grant SB070001.